Bulk Heterojunction Solar Cells from Poly(3-butylthiophene)/ Fullerene Blends: In Situ Self-Assembly of Nanowires, Morphology, Charge Transport, and Photovoltaic Properties

Hao Xin, Guoqiang Ren, Felix Sunjoo Kim, and Samson A. Jenekhe*

Departments of Chemical Engineering and Chemistry, University of Washington, Seattle, Washington 98195-1750

Received May 16, 2008. Revised Manuscript Received August 15, 2008

Bulk heterojunction solar cells based on blends of regioregular poly(3-butylthiophene) (P3BT) and phenyl-C_{61}-butyric acid methyl ester ($PC_{61}BM$) were created by in situ self-assembly of P3BT nanowires and the morphology and photovoltaic properties were investigated as a function of the blend composition. Transmission electron microscopy imaging of the blends revealed an interconnected network of P3BT nanowires of 11−15 nm width and 5−10 μm length and an amorphous continuous $PC_{61}BM$ phase. The photocurrent density, fill factor, and power conversion efficiency of the P3BT nanowire/$PC_{61}BM$ solar cells varied significantly with the blend composition whereas the open circuit voltage was relatively constant (570−610 mV). A maximum power conversion efficiency of 2.52% was achieved at a 1:0.5 (wt:wt) P3BT:$PC_{61}BM$ blend ratio. The hole mobilities in the P3BT nanowire/$PC_{61}BM$ blends measured by space-charge limited current and field-effect transistors were on the order of 1×10^{-3} cm^2/V s and a linear dependence of current density on light intensity was observed in the blend solar cells. These results demonstrate that in situ self-assembly of polymer semiconductor nanowires as active blend component is a promising approach to the rational control of the film morphology of bulk heterojunction solar cells.

Introduction

The excitonic nature of photovoltaic cells based on organic or polymer semiconductors[1] poses major challenges in developing them as practical, low-cost power sources derived from the sun.[2] The improved exciton dissociation accompanying the gradual evolution of the polymer solar cell architecture from the Schottky barrier single-layer[3] to the donor/acceptor bilayer heterojunction[4] and to the donor/acceptor bulk heterojunction (BHJ)[2,5,6] has seen the power conversion efficiency of devices rise from about 0.1%[3] to 1−1.5%[4] and 3−5%,[6,7] respectively. The BHJ polymer solar cell,[5−7] consisting of a binary blend or composite of a donor polymer and an acceptor material, such as fullerene, CdSe nanocrystals, TiO_2 nanoparticles, carbon nanotubes, an n-type polymer, or n-type small molecule, was introduced in 1995 to address the problem of small exciton diffusion lengths ($L_d = 5-20$ nm) in current organic/polymer semiconductors.[5] Optimized BHJ photovoltaic devices based on regioregular poly(3-hexylthiophene) (P3HT) and the [60]fullerene, [6,6]-phenyl-C_{61}-butyric acid methyl ester ($PC_{61}BM$) now have power conversion efficiencies of up to 4−5%.[6]

One of the difficult challenges in improving the performance of BHJ polymer solar cells is that the ideal two-phase, nanoscale, bicontinuous donor/acceptor morphology remains elusive because the thermodynamics and kinetics of blend

* Corresponding author. E-mail: Jenekhe@u.washington.edu.

(1) Gregg, B. A. *J. Phys. Chem. B* **2003**, *107*, 4688–4698.
(2) (a) Günes, S.; Neugebauer, H.; Sariciftci, N. S. *Chem. Rev.* **2007**, *107*, 1324–1338. (b) Thompson, B. C.; Frechet, J. M. J. *Angew. Chem., Int. Ed.* **2008**, *47*, 58–77. (c) Blom, P. W. M.; Mihailetchi, V. D.; Koster, L. J. A.; Markov, D. E. *Adv. Mater.* **2007**, *19*, 1551–1566. (d) Coakley, K. M.; McGehee, M. D. *Chem. Mater.* **2004**, *16*, 4533–4542. (e) Gledhill, S. E.; Scott, B.; Gregg, B. A. *J. Mater. Res.* **2005**, *20*, 3167–3179.
(3) (a) Antoniadis, H.; Hsieh, B. R.; Abkowitz, M. A.; Jenekhe, S. A.; Stolka, M. *Synth. Met.* **1994**, *62*, 265–271. (b) Marks, R. N.; Halls, J. J. M.; Bradley, D. D. C.; Friend, R. H.; Holmes, A. B. *J. Phys.: Condens. Matter* **1994**, *6*, 1379–1394.
(4) (a) Tang, C. W. *Appl. Phys. Lett.* **1986**, *48*, 183–185. (b) Sariciftci, N. S.; Braun, D.; Zhang, C.; Srdanov, V. I.; Heeger, A. J.; Stucky, G.; Wudl, F. *Appl. Phys. Lett.* **1993**, *62*, 585–587. (c) Halls, J. J. M.; Pichler, K.; Friend, R. H.; Moratti, S. C.; Holmes, A. B. *Appl. Phys. Lett.* **1996**, *68*, 3120–3122. (d) Jenekhe, S. A.; Yi, S. *Appl. Phys. Lett.* **2000**, *77*, 2635–2637. (e) Breeze, A. J.; Salomon, A.; Ginley, D. S.; Gregg, B. A.; Tillmann, H.; Horhold, H. H. *Appl. Phys. Lett.* **2002**, *81*, 3085–3087. (f) Alam, M. M.; Jenekhe, S. A. *Chem. Mater.* **2004**, *16*, 4647–4656.
(5) (a) Yu, G.; Gao, J.; Hummelen, J. C.; Wudl, F.; Heeger, A. J. *Science* **1995**, *270*, 1789–1791. (b) Halls, J. J. M.; Walsh, C. A.; Greenham, N. C.; Marseglia, E. A.; Friend, R. H.; Moratti, S. C.; Holmes, A. B. *Nature* **1995**, *376*, 498–500.
(6) (a) Li, G.; Shrotriya, V.; Huang, J. S.; Yao, Y.; Moriarty, T.; Emery, K.; Yang, Y. *Nat. Mater.* **2005**, *4*, 864–868. (b) Ma, W. L.; Yang, C. Y.; Gong, X.; Lee, K.; Heeger, A. J. *Adv. Funct. Mater.* **2005**, *15*, 1617–1622. (c) Kim, Y.; Cook, S.; Tuladhar, S. M.; Choulis, S. A.; Nelson, J.; Durrant, J. R.; Bradley, D. D. C.; Giles, M.; McCulloch, I.; Ha, C. S.; Ree, M. *Nat. Mater.* **2006**, *5*, 197–203.
(7) (a) Padinger, F.; Rittberger, R. S.; Sariciftci, N. S. *Adv. Funct. Mater.* **2003**, *13*, 85–88. (b) Mihailetchi, V. D.; Xie, H. X.; de Boer, B.; Koster, L. J. A.; Blom, P. W. M. *Adv. Funct. Mater.* **2006**, *16*, 699–708. (c) Nguyen, L. H.; Hoppe, H.; Erb, T.; Gunes, S.; Gobsch, G.; Sariciftci, N. S. *Adv. Funct. Mater.* **2007**, *17*, 1071–1078. (d) Kim, Y.; Choulis, S. A.; Nelson, J.; Bradley, D. D. C.; Cook, S.; Durrant, J. R. *Appl. Phys. Lett.* **2005**, *86*, 063502. (e) Erb, T.; Zhokhavets, U.; Hoppe, H.; Gobsch, G.; Al-Ibrahim, M.; Ambacher, O *Thin Solid Films* **2006**, *511−512*, 483–485. (f) Yang, X. N.; Loos, J.; Veenstra, S. C.; Verhees, W. J. H.; Wienk, M. M.; Kroon, J. M.; Michels, M. A. J.; Janssen, R. A. J. *Nano Lett.* **2005**, *5*, 579–583. (g) Blouin, N.; Michaud, A.; Gendron, D.; Wakim, S.; Blair, E.; Neagu-Plesu, R.; Belletête, M.; Durocher, G.; Tao, Y.; Leclerc, M. *J. Am. Chem. Soc.* **2008**, *130*, 732–742.

10.1021/cm801324m CCC: $40.75
Published on Web 09/23/2008

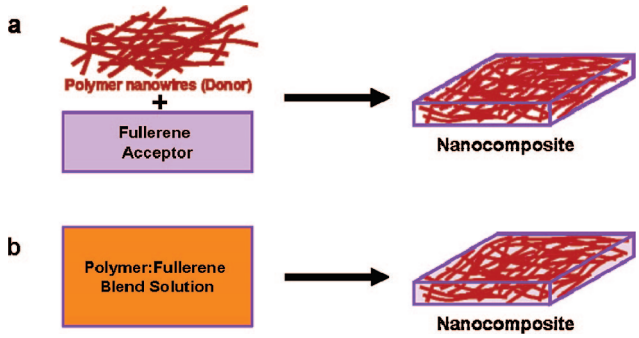

Figure 1. Illustration of the preparation of nanocomposites of polymer (P3BT) nanowires and fullerene via (a) preassembled polymer nanowires and (b) in situ self-assembly of polymer nanowires.

phase separation cannot be controlled since numerous variables are involved.[2,6] The time-dependent Ostwald ripening or domain coarsening phenomena in phase-separated polymer blends are also major sources of instability and poor durability of current BHJ polymer solar cells.[2a,b,8] Some approaches to controlling the nanoscale film morphology of P3HT/fullerene blend solar cells have recently been reported,[9] including solution precipitation of P3HT nanofibers[9a] and the use of a mixed solvent as a means to control aggregation of P3HT.[9b] Innovations in materials, materials processing, and device architectures are necessary to significantly improve the performance of BHJ polymer solar cells.

Recently, we discovered that highly efficient BHJ solar cells could be achieved by using preassembled poly(3-butylthiophene) (P3BT) nanowires (NWs) as the donor component along with $PC_{61}BM$ or $PC_{71}BM$ as the acceptor as illustrated in Figure 1a.[10] TEM imaging of the P3BT NWs showed that they had a width of 9 ± 1 nm, which is within the exciton diffusion range. Moreover, the nanowires showed higher field-effect hole mobility (8.0×10^{-3} cm^2/V s) in composite film with $PC_{61}BM$ than that obtained from P3BT:$PC_{61}BM$ blend film (3.8×10^{-5} cm^2/V s). These features indicate the P3BT NWs constitute an ideal donor component for enhanced exciton diffusion and charge transport in BHJ solar cells. Indeed, the performance achieved from the P3BT NW/$PC_{71}BM$ composite (PCE = 3.0%) solar cells was 1 order of magnitude higher compared with prior results from thermally induced phase-separated P3BT:fullerene blend solar cells.[10] The many advantages of the polymer semiconductor NW approach to the BHJ solar cell include: (a) a rational control of the morphology; (b) the polymer NWs with widths of 10−20 nm and lengths of microns have sizes that are perfectly matched to the exciton diffusion lengths; (c) ultralarge donor/acceptor interfacial area for efficient exciton dissociation; (d) an electrically bicontinuous morphology is achieved a priori; (e) high carrier mobilities and high absorption coefficient are achieved because of the high crystallinity of the self-assembled NWs; (f) ease of production of devices on plastic substrates and scalability to large areas; (g) it avoids the difficulties of blend phase-separation phenomena, including domain coarsening and time-dependent instability.

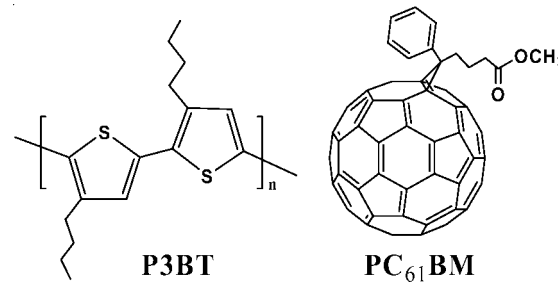

Figure 2. Chemical structures of regioregular P3BT and $PC_{61}BM$.

In this paper, we demonstrate the use of in situ self-assembly of polymer semiconductor NWs in blends with $PC_{61}BM$ to create efficient BHJ polymer solar cells. An attractive feature of the present approach, illustrated in Figure 1b, is that it simplifies and collapses the previously separate processes of preparing the polymer semiconductor NWs and the blending with fullerenes[10] into a single process. The P3BT NW:$PC_{61}BM$ blend film morphology was investigated by transmission electron microscopy (TEM) and atomic force microscopy (AFM). Electrical characterization of the P3BT NW:$PC_{61}BM$ blend solar cells, under AM1.5 white light (1 sun = 100 mW/cm^2) illumination, as a function of blend composition found a peak in the power conversion efficiency (2.52%) at the 1:0.5 P3BT:$PC_{61}BM$ ratio. The molecular structures of regioregular P3BT and $PC_{61}BM$ are shown in Figure 2.

Experimental Section

Poly(3-butylthiophene) (P3BT, 97% head-to-tail regioregularity) was purchased from Aldrich. The [60] fullerene, [6,6]-phenyl-C_{61}-butyric acid methyl ester (PCBM, >99.5%), was obtained from American Dye Source, Inc. (Quebec, Canada). All the chemicals were used as received without further purification. Poly(3,4-ethylenedioxythiophene):poly(styrene sulfonate) (PEDOT) (Baytron P VP AI 4083) was purchased from H. C. Stark (Newton, MA) and diluted with deionized water (PEDOT:H_2O = 4:1 v/v) and passed through a 0.45 μm filter before spin-coating.

P3BT and $PC_{61}BM$ solutions were prepared by dissolving them separately in nitrogen-degassed 1,2-dichlorobenzene (ODCB). The P3BT solution (10 mg/mL) was heated at 90−100 °C under stirring for 24 h to obtain a completely dissolved hot solution, which was filtered by using a 0.45 μm filter. $PC_{61}BM$ solutions (60 mg/mL) were stirred at 40 °C overnight and passed through a 0.2 μm filter. The P3BT:$PC_{61}BM$ blends were made by mixing the just-filtered hot P3BT solution with PCBM solution at different ratios. The concentration of P3BT:$PC_{61}BM$ blends with the weight ratio of 1:2, 1:1, 1:0.5, and 1:0.25 correspond to a concentration of 22.5, 17.1, 13.8, and 12.0 mg/mL, respectively. The blend solutions were stored in a glovebox for P3BT nanowires to self-assemble before they were used for fabricating solar cells and/or for characterization purposes.

Solar cells were fabricated by first spin-coating a PEDOT buffer layer on top of ITO-coated glass substrates (10 Ω/□, Shanghai B. Tree Tech. Consult Co., Ltd., Shanghai, China) at 1500 rpm for 60 s and dried at 150 °C for 10 min under vacuum. The thickness

(8) Campoy-Quiles, M.; Ferenczi, T.; Agostinelli, T.; Etchegoin, P. G.; Kim, Y.; Anthopoulos, T. D.; Stavrinou, P. N.; Bradley, D. D. C.; Nelson, J. *Nat. Mater.* **2008**, *7*, 158–164.
(9) (a) Berson, S.; Bettignies, R. D.; Bailly, S.; Guillerez, S. *Adv. Mater.* **2007**, *17*, 1377–1384. (b) Moule, A. J.; Meerholz, K. *Adv. Mater.* **2008**, *20*, 240–245.
(10) Xin, H.; Kim, F. S.; Jenekhe, S. A. *J. Am. Chem. Soc.* **2008**, *130*, 5424–5425.

of PEDOT was around 60 nm. The active blend layer was spin-coated on top of the PEDOT layer from the P3BT:$PC_{61}BM$ blend at a speed of 1000 rpm for 30 s and annealed on a hot plate at 130 ± 10 °C for 10 min in a glovebox. Although P3BT:$PC_{61}BM$ blends with a different composition had a different solution concentration, films spin-coated under the same condition had a similar thickness ~200−230 nm. This is because of the high viscosity of the blend solutions which contain P3BT nanowires. After being cooled, the substrates were taken out of the glovebox and loaded in a thermal evaporator (BOC Edwards, 306) for the deposition of the cathode. The cathode consisting of 1.0 nm LiF and 80 nm aluminum layers was sequentially deposited through a shadow mask on top of the active layers in a vacuum of 8×10^{-7} Torr. Each substrate contained 5 solar cells with an active area of 3.57 mm^2. Devices for space-charge limited current (SCLC) measurement were fabricated similar to those of solar cells. The main difference is that in order to facilitate hole-only injection and transport, gold electrode was deposited instead of the lithium fluoride (LiF) and aluminum cathode in the solar cells.

Film thickness was measured by an Alpha-Step 500 profilometer (KLA-Tencor, San Jose, CA). Current−voltage characteristics of both solar cells and SCLC devices were measured using a HP4155A semiconductor parameter analyzer (Yokogawa Hewlett-Packard, Tokyo). The light intensity of AM1.5 sunlight from a filtered Xe lamp was controlled by using a set of neutral density filters. The SCLC characteristics were measured under dark conditions. All the characterization steps were carried out under ambient laboratory air.

Field-effect transistors were fabricated on heavily doped (n-type) silicon substrates with thermally grown silicon dioxide (300 nm). Doped silicon acted as common gate electrode and silicon dioxide as gate insulator. Source and drain electrodes were patterned on top of the substrates by using photolithography and thermal evaporation of 2 nm thick chromium and 60 nm thick gold. The bottom-contact/bottom-gate devices had channel width of 800 μm and length of 20 μm. Substrates were cleaned by ultrasonication with acetone and isopropyl alcohol, and purged with argon. Octyltriethoxysilane (OTS-8) monolayer was deposited on the substrates in vacuum desiccator at 60 °C for more than 6 h, and cross-linked by placing on hot plate at 120 °C for 20 min. In situ nanowire suspensions with various compositions were spun on the substrates (2000 rpm, 60 s). Devices were dried under the same conditions as described above for solar cells. Electrical characteristics of the field-effect transistors were measured on a Keithley 4200 semiconductor characterization system (Keithley Instruments Inc. Cleveland, OH). The field-effect mobility was calculated from the equation for saturation region, following our previous reported approaches.[11] All the measurements were done under dark condition in air.

Transmission electron microscopy (TEM) images were acquired on a Phillips EM420 microscope at 100 kV with objective aperture in to enhance the contrast. P3BT:$PC_{61}BM$ blend films for TEM imaging were prepared from solutions diluted about 10 times by the same ODCB solvent. The samples for TEM acquisition were prepared by dropping a small amount of the diluted P3BT:$PC_{61}BM$ blend solution onto a TEM grid and allowed to dry in a glovebox overnight. Measurement of the width (diameter) of the nanowires was made by using ImageJ software (v 1.39, NIH) to analyze the TEM images. Atomic Force Microscopy (AFM) images were measured from the same film as in the solar cell devices by using a Dimension 3100 Scanning Probe Microscope (Veeco Instruments Inc., Woodbury, NY) in standard tapping mode.

UV−vis absorption spectra were recorded on a Perkin-Elmer model Lambda 900 UV/vis/near-IR spectrophotometer. The P3BT films for absorption measurements were spin-coated on glass slides, whereas P3BT:$PC_{61}BM$ blend films were spin-coated on top of ITO/PEDOT substrates. All blend films were annealed under the same conditions as those of the photovoltaic devices.

Results and Discussion

In Situ Self-Assembly of P3BT Nanowires. In our previous report,[10] P3BT/fullerene ($PC_{61}BM$ or $PC_{71}BM$) nanocomposite bulk heterojunction solar cells were prepared by a process in which the P3BT nanowires (NWs) were self-assembled separately prior to the mixing with the fullerene as illustrated in Figure 1a. In the present study, we explored the possibility of combining those two separate steps—assembly of P3BT NWs in a separate solution followed by mixing with the fullerene—into one process whereby the assembly of the P3BT NWs takes place in situ, in the presence of the fullerene (Figure 1b). The key result of this study is that this can indeed be done. We found that when a hot (80−90 °C) P3BT:$PC_{61}BM$ blend solution cools down to room temperature and stands for some time, self-assembly of P3BT NWs occurs in the blend solution over time in very similar ways to the assembly of NWs in a pure P3BT solution.

Evidence of the in situ self-assembly of P3BT NWs in P3BT:$PC_{61}BM$ blend solutions comes from the solution viscosity, absorption spectroscopy, and the morphology and photovoltaic properties of films prepared from the blend solutions. The P3BT:$PC_{61}BM$ blend solution viscosity was observed to increase substantially with time, reaching a plateau in about 26 h. Transmission electron microscopy (TEM) imaging, absorption spectroscopy, and photovoltaic measurements similarly indicated that the in situ self-assembly of P3BT NWs was complete within about 26 h. Therefore, all the P3BT:$PC_{61}BM$ blends used in detailed studies as a function of composition were done at the 26 h mark of the in situ self-assembly of P3BT NWs.

Morphology of P3BT:PCBM Blends. Figure 3 shows the bright field TEM images of blend films with P3BT:$PC_{61}BM$ compositions of 1:2 and 1:0.25. Both films show a network of P3BT NWs with lengths in the 5−10 μm range. An image analysis based on 200 random measurements of the widths (or diameters) seen in the TEM images of larger magnifications, gave a width range of 11−15 nm; the width of the P3BT NWs observed here is slightly larger than those formed in ODCB solution without $PC_{61}BM$.[8] The P3BT NWs have a very high aspect ratio (length/width) of about 500−900.

An interconnected P3BT nanowire network can be clearly seen in both films (Figure 3), regardless of the blend composition. No obvious $PC_{61}BM$ crystals are observed, indicating the amorphous nature of the $PC_{61}BM$ phase in the blend films. The observed morphology of the P3BT NW/$PC_{61}BM$ blends is quite different from those commonly observed in thermally induced phase separation of P3HT:$PC_{61}BM$ blend films, in which P3HT formed globular/fibrillar

(11) (a) Babel, A.; Jenekhe, S. A. *J. Am. Chem. Soc.* **2003**, *125*, 13656–13657. (b) Babel, A.; Jenekhe, S. A. *J. Phys. Chem. B* **2003**, *107*, 1749–1754. (c) Babel, A.; Jenekhe, S. A. *Macromolecules* **2003**, *36*, 7759–7764.

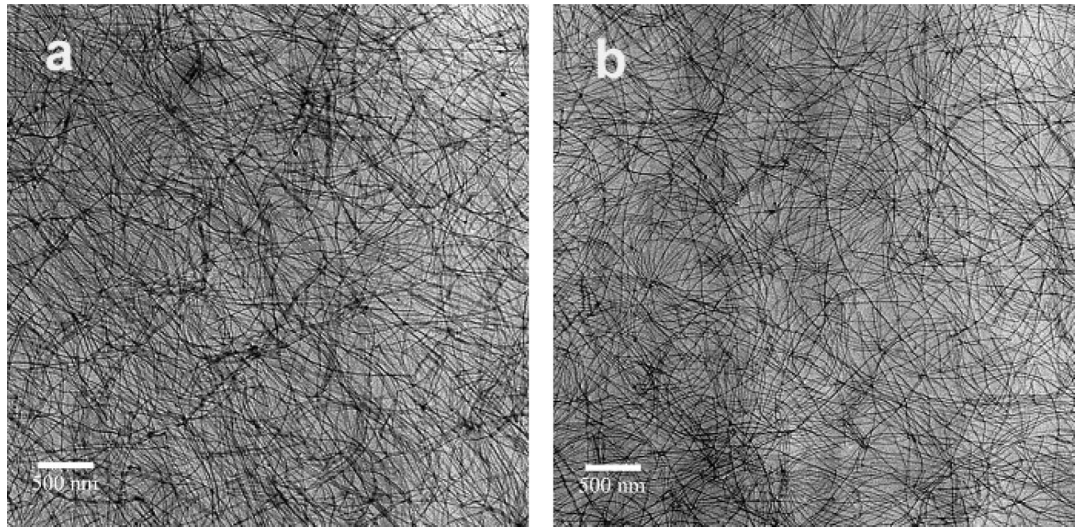

Figure 3. TEM images of P3BT:$PC_{61}BM$ blends at compositions of (a) 1:2 and (b) 1:0.25. The scale bar is 500 nm in both (a) and (b).

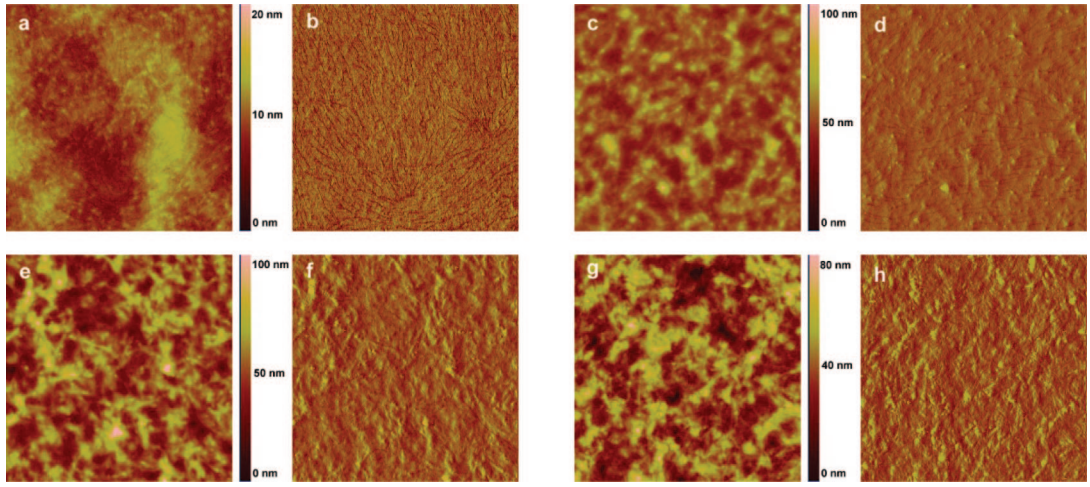

Figure 4. (a, c, e, g) Tapping mode AFM topography and (b, d, f, h) phase images of P3BT:$PC_{61}BM$ blend films with different compositions: (a, b) 1:2, (c, d) 1:1, (e, f) 1:0.5, and (g, h) 1:0.25. The area is 5 μm $\times$ 5 μm for all the images. The films were spin-coated onto ITO/PEDOT substrates and annealed at 130 °C for 10 min.

structures together with nano- or microcrystalline $PC_{61}BM$, depending on the blend composition and annealing conditions.[7]

We note that the P3BT:$PC_{61}BM$ blend solutions were diluted about 10 times to obtain sufficiently thin films for TEM imaging. Therefore, we expect the P3BT NW density in the actual photovoltaic devices was substantially higher than that observed in the TEM images in Figure 3. In addition, P3BT NW density in the devices varies with blend composition; blends with a higher fraction of fullerene had a lower P3BT NW density. Thus, in the four P3BT:$PC_{61}BM$ blends studied in this work, the 1:2 P3BT:$PC_{61}BM$ blend had the lowest P3BT NW density, whereas the 1:0.25 P3BT:$PC_{61}BM$ blend had the highest P3BT NW density. We anticipate that this variation in P3BT NW density will have impact on the photovoltaic properties.

Figure 4 shows the AFM images of blend films spin-coated on top of ITO/PEDOT substrates and annealed at 130 $\pm$ 10 °C for 10 min. In all the films of different blend compositions, long P3BT nanowires, similar to those seen in the TEM images (Figure 3) are visible in the phase images. However, the surface morphology seen in the topographic AFM images is quite different as the blend composition changes. In the film which contains the most $PC_{61}BM$ (P3BT:$PC_{61}BM$ = 1:2), a continuous $PC_{61}BM$ phase with only a small number of nanowires is seen. The film surface is quite smooth with a root mean-square (rms) roughness of 1.68 nm (images a and b in Figure 4). As the $PC_{61}BM$ fraction decreases, such as in films with P3BT: $PC_{61}BM$ ratios of 1:1 and 1:0.5, more and more P3BT nanowires are visible from the surface topography images while $PC_{61}BM$ still forms a continuous phase. The surface roughness in these films is dramatically increased to rms of 7.90 and 13.2 for the 1:1 and 1:0.5 blends, respectively, and many $PC_{61}BM$ crystal domains with tens of nanometer size are also clearly observed (images d and f in Figure 4). Further decrease of the $PC_{61}BM$ fraction results in a blend film (P3BT:$PC_{61}BM$ = 1:0.25) in which the P3BT nanowires are highly interconnected, whereas $PC_{61}BM$ phase exists as isolated domains instead of a continuous phase. The surface roughness of this film has an rms of 11.2 nm.

The morphology of the P3BT:$PC_{61}BM$ blends revealed by TEM and AFM phase images is essentially the same except the increased P3BT NW density in the AFM phase images. However, the different features seen in the AFM topographic

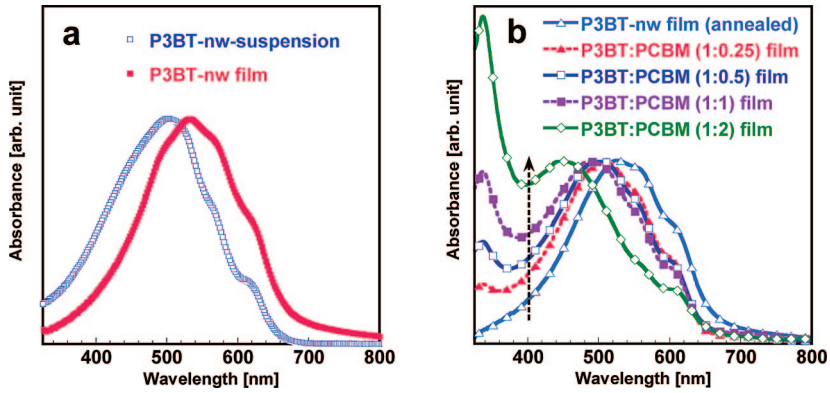

Figure 5. (a) UV−vis absorption spectra of P3BT nanowire suspension in ODCB and as a spin-coated film on glass. (b) Normalized absorption spectra of P3BT-nw and P3BT-nw:$PC_{61}BM$ blend films of different compositions. All the films were annealed at 130 °C for 10 min. P3BT-nw film was spin-coated on a glass slide, whereas P3BT-nw:$PC_{61}BM$ blend films were spin-coated on top of ITO/PEDOT substrates.

images can be accounted for by effects of the annealing. It was confirmed that without annealing the AFM topographic images showed similar interconnected network of P3BT NWs as that seen in the TEM images; in this case, $PC_{61}BM$ was homogeneously dispersed in between the P3BT NWs (not shown) and the overall morphology was similar to that in preformed P3BT NW:$PC_{61}BM$ composite films.[10]

The bulk and surface morphologies, observed in the present P3BT:$PC_{61}BM$ blends are dramatically different from those commonly observed in thermally induced phase-separated P3HT:$PC_{61}BM$ blends in which both polymer and $PC_{61}BM$ exist as globular and crystalline domains.[2a,7b−e] Thermally induced phase separation in polymer-fullerene blend is thought to involve two steps: (1) the aggregation and crystallization of the polymer accompanied by free diffusion of the $PC_{61}BM$ molecules; and (2) slow crystallization of the $PC_{61}BM$ phase.[2a,d] Simultaneous lateral and vertical phase segregation occur during the annealing process.[8] In the case of our P3BT:$PC_{61}BM$ blends, diffusion of the polymer molecules does not occur in the films during the annealing process since they are already tied down in the assembled NWs. The $PC_{61}BM$ molecules, however, can diffuse laterally and vertically.

Optical Absorption. The absorption spectra of a suspension of P3BT NWs in ODCB and a spin-coated film of P3BT NWs are shown in Figure 5a. The P3BT NW suspension shows three absorption peaks at 502, 563, and 616 nm. Obviously, the later two vibronic peaks are due to the strong $\pi-\pi$ stacking within the assembled P3BT NWs.[12,13] As expected, the two vibronic features at 563 and 616 nm in the thin film are at the same wavelengths as in the absorption spectrum of the P3BT NW suspension. The main absorption peak in the film at 532 nm is red-shifted from that observed in the suspension due to the stronger internanowire interaction in the condensed film. We note that the absorption of the P3BT NWs as a thin film is 10 nm red-shifted compared to the reported absorption maximum of solid-state thin film of P3BT in the literature,[14] in which the three peaks were found at 522, 556, and 605 nm, respectively, indicating a more ordered structure in the P3BT nanowires. The optical bandgap (E_g) of the P3BT NWs deduced from the onset of the absorption spectra is 1.85 eV (670 nm) in both suspension and thin film.

Figure 5b shows the normalized thin film absorption spectra of the P3BT NWs and P3BT:$PC_{61}BM$ blends. The P3BT NW film was spin-coated on a glass slide whereas the blend films were spin-coated on top of ITO/PEDOT substrates. All the films were annealed at 130 °C for 10 min. The absorption spectrum of annealed P3BT NW film is identical to the nonannealed one (Figure 5a). The absorption of P3BT NWs is progressively blue-shifted with the loading of $PC_{61}BM$, the main absorption peak at 532 nm in the pure film is gradually blue-shifted to 450 nm in the 1:2 P3BT:$PC_{61}BM$ film. This blue-shift can be explained by the reduced internanowire interaction disrupted by the presence of $PC_{61}BM$.[15] However, the characteristic vibronic features at 563 and 616 nm, due to the $\pi-\pi$ stacking within the P3BT NWs, show no obvious change even at the highest $PC_{61}BM$ loading (P3BT:$PC_{61}BM$ = 1:2). This shows that ordered structure of the P3BT NWs is not disrupted in the blend films.

Charge-Transport Properties. Charge-carrier motilities in the P3BT:$PC_{61}BM$ blends were evaluated by both space-charge limited current (SCLC)[16] and organic field-effect transistors (OFETs).[11] Figure 6a shows the relationship between dark-current density (J) and voltage (V) in the hole-only devices of P3BT:$PC_{61}BM$ blends of different composition. The $J-V$ data were analyzed by using the nonlinear least-squares fitting to the modified Mott−Gurney equation (eq 1),[16]

$$J = \frac{9}{8}\varepsilon\varepsilon_0\mu\frac{V^2}{L^3}\exp\left(\frac{0.89\beta}{\sqrt{L}}\sqrt{V}\right) \quad (1)$$

where J is the current density, V is the applied voltage, L is the thickness of active layer, μ is the mobility, ε is the relative permittivity, ε_0 is the permittivity of free space, and β is the field-activation factor.[16] The solid lines in Figure 6a represent the fitting curves using this model. The zero-field mobilities

(12) McCullough, R. D.; Tristram-Nagle, S.; Williams, S. P.; Lowe, R. D.; Jayaraman, M. *J. Am. Chem. Soc.* **1993**, *115*, 4910–4911.
(13) Cornil, J.; Beljonne, D.; Calbert, J. P.; Bredas, J. L. *Adv. Mater.* **2001**, *13*, 1053–1067.
(14) Chen, T. A.; Wu, X. M.; Rieke, R. D. *J. Am. Chem. Soc.* **1995**, *117*, 233–244.
(15) Li, G.; Yao, Y.; Yang, H.; Shrotriya, V.; Yang, G.; Yang, Y. *Adv. Funct. Mater.* **2007**, *17*, 1636–1644.
(16) Murgatroyd, P. N. *J. Phys. D: Appl. Phys.* **1970**, *3*, 151–156.

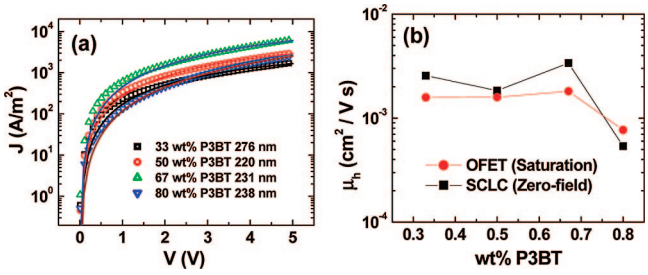

Figure 6. (a) Experimental dark-current density−voltage curves for P3BT-nw:$PC_{61}BM$ hole only devices as a function of blend composition (wt % P3BT). The solid lines represent the fit using a model of single carrier SCL current with field-dependent mobility. (b) Comparison of the SCLC and field-effect hole motilities of P3BT-nw:$PC_{61}BM$ nanocomposites versus composition (wt % P3BT).

of the P3BT:$PC_{61}BM$ blends were calculated to be 2.56×10^{-3}, 1.84×10^{-3}, 3.38×10^{-3}, and 5.37×10^{-4} cm^2/V s for the 1:2, 1:1, 1:0.5, and 1:0.25 compositions, respectively, and shown in Figure 6b. These SCLC hole mobilities of the P3BT nanowires in the P3BT/$PC_{61}BM$ blends are 1 order of magnitude higher than that of P3HT in annealed P3HT/$PC_{61}BM$ (1:1) blends, which is about 2×10^{-4} cm^2/V s.[7b] The lower SCLC hole mobility in the 1:0.25 P3BT:$PC_{61}BM$ blend may be caused by "grain boundary" effects between the P3BT nanowires due to the high density of wires. The SCLC hole mobility of a film of pure P3BT nanowires (without $PC_{61}BM$) measured under the same condition is 1.35×10^{-4} cm^2/V s. We note that the hole mobilities of the P3BT:$PC_{61}BM$ blends show a negative electric field dependence. The β values obtained from P3BT:$PC_{61}BM$ blends with a composition of 1:2, 1:1, 1:0.5, and 1:0.25 were -3.89×10^{-4}, -3.12×10^{-4}, -2.48×10^{-4}, and -5.45×10^{-5}, respectively. This phenomenon has been observed in pure polythiophene[17] and P3HT:$PC_{61}BM$ blends[18] and has been attributed to the small energetic but large spatial disorder in the materials.

Field-effect mobility was calculated from the standard equation for the saturation region in field-effect transistors.[11] The field-effect hole mobility of P3BT:$PC_{61}BM$ blends ranged from 1.6×10^{-3} cm^2/V s for the 1:2 and 1:1 blends to 7.7×10^{-4} cm^2/V s for the 1:0.25 blend (Figure 6b). The OFET mobility of the in situ formed P3BT nanowires in the 1:1 P3BT:$PC_{61}BM$ blend is in the same order as the preformed P3BT nanowires in nanocomposite with fullerenes.[10] The field-effect electron mobilities of P3BT:$PC_{61}BM$ blends were not observed because our measurements were all done in air.

Interestingly, as shown in Figure 6b, the OFET mobilities for the same P3BT:$PC_{61}BM$ nanocomposites show a remarkable similarity with the SCLC data. We interpret the agreement between the OFET and SCLC carrier mobility data to mean that the morphology of the BHJ thin films is uniform both horizontally and vertically, although the orientation of the polymer NWS is random in the films, a unique consequence of the NW architecture of the nanocomposites. The hole mobilities of the P3BT nanowires in the P3BT:$PC_{61}BM$ blends are comparable to the electron mobility of $PC_{61}BM$,[2a] so balanced charge transport would be expected in the P3BT:$PC_{61}BM$ blend solar cells if the measurements are done in an inert atmosphere.

Photovoltaic Properties. Photovoltaic cells incorporating P3BT:$PC_{61}BM$ blends as the active layer were fabricated as 3.57 mm^2 area and tested under a 100 mW/cm^2 AM1.5 sunlight illumination in ambient air. The device structure, ITO/PEDOT/P3BT:$PC_{61}BM$/LiF/Al, is illustrated in the inset of Figure 7a. The current−voltage curves of the P3BT:$PC_{61}BM$ blend solar cells at different blend compositions are shown in Figure 7. The photovoltaic parameters, the short-circuit current density (J_{sc}), the open circuit voltage (V_{oc}), the fill factor (FF), and the power conversion efficiency (PCE) together with the hole mobilities are summarized in Table 1. The series and parallel (shunt) resistances respectively deduced by the inverse gradient of the $J-V$ curves[19] at the open circuit and the short circuit of the $J-V$ curves are also given in Table 1. It is obvious that the performance of the photovoltaic cells greatly depends on the blend composition. At a P3BT:$PC_{61}BM$ blend ratio of 1:2, a power conversion efficiency of 1.11% was observed. When the blend ratio increased to 1:1, the efficiency increased to 2.39%. The best performance was achieved at a P3BT:$PC_{61}BM$ ratio of 1:0.5, in which $J_{sc} = 9.01$ mA/cm^2, $V_{oc} = 0.60$ V, FF = 0.47, and a power conversion efficiency of 2.52% were obtained. Further increase of the relative amount of P3BT NWs to P3BT:$PC_{61}BM$ ratio of 1:0.25, results in a dramatic decrease of the efficiency to 0.78%, although the V_{oc} increased slightly to 0.61 V, the highest among the four compositions.

These photovoltaic devices based on P3BT NWs generally had excellent diode characteristics. For example, the 1:0.5 P3BT:$PC_{61}BM$ blend cell, whose current−voltage characteristics are shown in Figure 7b, showed very high rectification ratios of 2.9×10^3 in the dark at ±0.60 V and 2.6×10^4 at ±0.85 V. The other blend photovoltaic cells similarly had excellent rectification ratios. The excellent diode characteristics can be understood given the extremely large shunt resistance. From the dark $J-V$ curves in Figure 7b, the shunt resistances are calculated to be in the range of 1×10^5 to 1×10^6 Ω cm^2. We note that under illumination, the shunt resistances (r_p) are dramatically decreased (Table 1), the reason for the light-dependent shunt resistance is not clear.

To gain insight into the operation of these P3BT:$PC_{61}BM$ blend solar cells, we studied the light-intensity dependence of the photocurrent. The $J-V$ characteristics of the 1:0.5 P3BT:$PC_{61}BM$ solar cells under illumination of different light intensities are shown in Figure 8a. The current density and open circuit voltage as a function of light intensity for the four composition solar cells are shown in panels b and c in Figure 8, respectively. It is obvious that J_{sc} of all four compositions show linear dependence on the light intensity, which indicates no space charge is formed[2c,7b,19] and the short-circuit current density loss is dominated by the monomolecular recombination.[20] The space charge free carrier transport can be understood given the high hole mobilities of the P3BT nanowires within the blends. Such mobilities

(17) (a) Mozer, A. J.; Sariciftci, N. S. *Chem. Phys. Lett.* **2004**, *389*, 438–442. (b) Mozer, A. j.; Sariciftci, N. A.; Pivrikas, A.; Osterbacka, R.; Juska, G.; Brassat, L.; Bassler, H. *Phys. Rev. B* **2005**, *71*, 035214.
(18) Huang, J.; Li, G.; Yang, Y. *Appl. Phys. Lett.* **2005**, *87*, 112105.
(19) Moliton, A; Nunzi, J.-M. *Polym. Int.* **2006**, *55*, 583–600.
(20) Riedel, I.; Parisi, J.; Dyakonov, V.; Lutsen, L.; Vanderzande, D.; Hummelen, J. C. *Adv. Funct. Mater.* **2004**, *14*, 38–44.

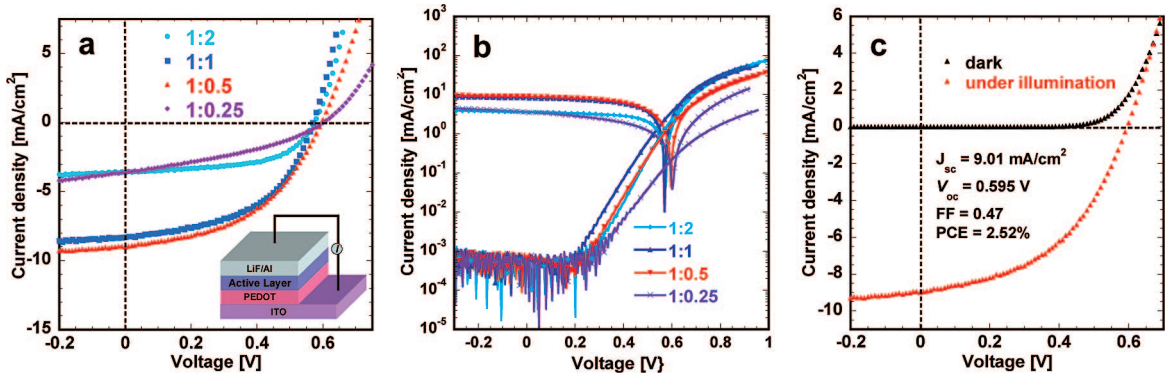

Figure 7. (a) The current−voltage characteristics of P3BT-nw:$PC_{61}BM$ blend solar cells with a structure of ITO/PEDOT/P3BT:$PC_{61}BM$/LiF/Al at different blend ratios, measured under AM1.5 white light illumination at 100 mW/cm.^{2} Inset: schematic structure of the solar cell device. (b) The current−voltage curves of P3BT-nw:$PC_{61}BM$ in (a) and their dark curves plotted in semilogarithmic format. (c) The current−voltage curves of the P3BT:$PC_{61}BM$ (1:0.5 wt:wt) blend device in the dark and under 100 mW/cm^2 illumination.

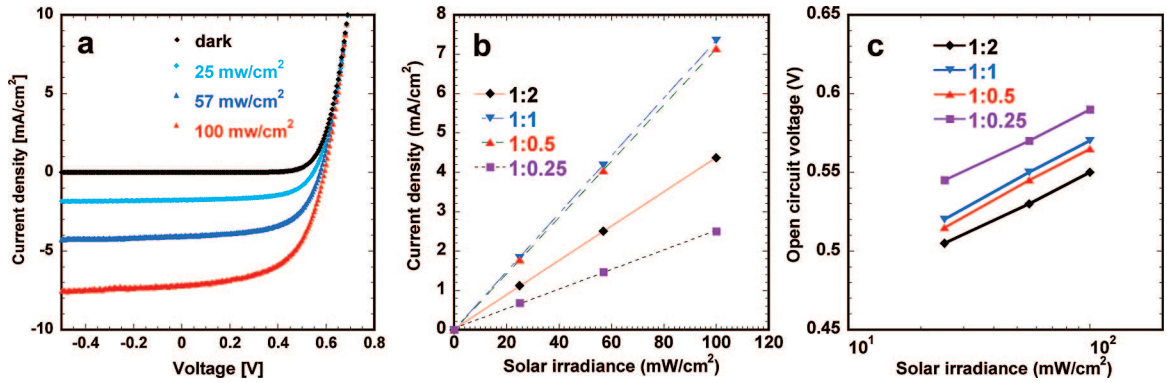

Figure 8. (a) Current density−voltage characteristics of P3BT:$PC_{61}BM$ (1:0.5) blend solar cell in the dark and under AM1.5 white light illumination at different light intensities. (b) The current density of the P3BT:$PC_{61}BT$ solar cells as a function of the light intensity. (c) Open circuit voltage of the P3BT:$PC_{61}BT$ solar cells as a function of the light intensity.

Table 1. Summary of Photovoltaic Properties of P3BT:$PC_{61}BM$ Blend Solar Cells

P3BT:$PC_{61}BM$ (wt %)	$\mu_{h\text{-SCLC}}$ (cm^2/V s)	$\mu_{h\text{-FET}}$ (cm^2/V s)	r_s (Ω cm^2)	r_p (Ω cm^2)	J_{sc} (mA/cm^2)	V_{oc} (V)	FF	PCE (%)
1:2	2.56×10^{-3}	1.6×10^{-3}	21.1	1063	3.45	0.57	0.56	1.11
1:1	1.84×10^{-3}	1.6×10^{-3}	13.5	467	8.29	0.57	0.51	2.39
1:0.5	3.38×10^{-3}	1.8×10^{-3}	18.5	413	9.01	0.60	0.47	2.52
1:0.25	5.37×10^{-4}	7.7×10^{-4}	54.5	315	3.62	0.61	0.35	0.78

are comparable to reported electron mobility of $PC_{61}BM$.[2b] However, since our devices were measured in air, the generated charge carriers, especially electron may be trapped by impurities such as oxygen, water, and recombined with opposite charge,[20] leading to low solar cell efficiency. The trapping and monomolecular recombination mechanism is valid if we consider that field-effect electron mobility could not be observed in the OFETs. Because the short-circuit current density is proportional to the light intensity, the V_{oc} increases logarithmically with the light intensity as expected (Figure 8c).[20,21]

To further understand the relationship between the blend composition and the photovoltaic properties, we plotted the dependence of J_{sc}, V_{oc}, FF, and PCE as a function of wt % P3BT (Figure 9). It should be noted that P3BT:$PC_{61}BM$ weight ratios of 1:2, 1:1, 1:0.5, and 1:0.25 correspond to 33, 50, 67, and 80 wt % P3BT, respectively. As seen in Figure 9a, the short-circuit current density as a function of composition (wt % P3BT) has a peak at approximately 66% P3BT and then at high fraction (80%), it dramatically decreased to 3.62 mA/cm^2. Because the hole mobility and the series resistances are comparable from the 1:2 to the 1:0.5 P3BT:$PC_{61}BM$ blend ratio, the small current density (3.45 mA/cm^2) at low P3BT fraction (33%) can be understood as a consequence of poor absorption because P3BT is the main absorber harvesting light in the devices. When the P3BT fraction is 80%, the series resistance dramatically increases to 54.5 Ω cm^2 from 18.5 Ω cm^2 in the 1:0.5 P3BT:$PC_{61}BM$ blend and hence the photocurrent in this cell should largely be limited by the high series resistance. We note that the series resistances observed in P3BT:$PC_{61}BM$ solar cells are much higher than those of annealed P3HT:$PC_{61}BM$ blend films, which are less than 8 Ω cm^2.[6b,22] The reason for the high series resistance of the P3BT:$PC_{61}BM$ blends is not clear. Possible reasons include the thick active layer (~220 nm) and the large film roughness of the blend film surface as revealed by the AFM images (Figure 4), which might lead to high contact resistance.

(21) Mengesha, U.; Yohammens, T. *Sol. Energy Mater. Sol. Cells* **2006**, *90*, 3508–3519.

(22) Chu, C. W.; Yang, H.; Hou, W. J.; Huang, J.; Li, G.; Yang, Y. *Appl. Phys. Lett.* **2008**, *92*, 103306.

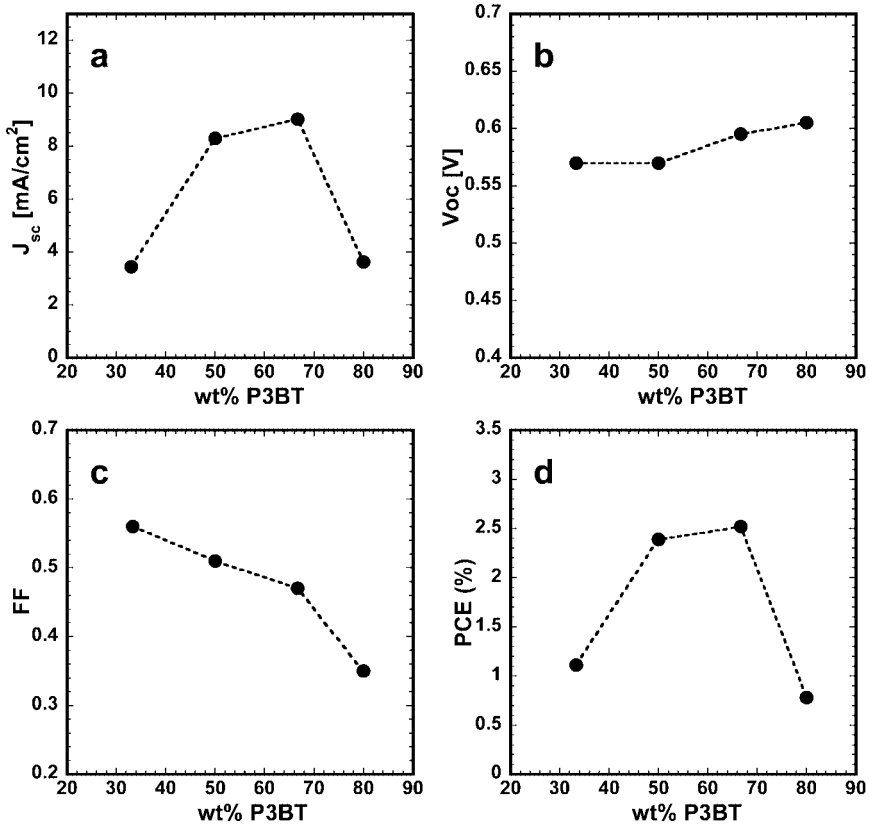

Figure 9. Dependence of (a) the short-circuit density J_{sc}, (b) the open circuit voltage V_{oc}, (c) the fill factor FF, and (d) the power conversion efficiency PCE of P3BT:$PC_{61}BM$ blend solar cells on blend composition (wt % P3BT). All measurements were done under AM1.5 white light illumination at 100 mW/cm.[2]

The open circuit voltage, V_{oc}, in all the photovoltaic devices is found to be quite stable (Figure 9b). It increases from 0.57 V at 33% P3BT to 0.61 V at 80% P3BT (Figure 7b). In contrast, V_{oc} in reported P3HT:$PC_{61}BM$ blend devices was found to be more dependent on the blend composition, increasing by 0.1 V when the $PC_{61}BM$ loading changed from 20% to 80%.[23] The large variation of V_{oc} in P3HT:$PC_{61}BM$ blend devices has been explained in terms of the disruptive role of $PC_{61}BM$ in the intermolecular packing of P3HT, leading to different effective bandgaps of P3HT in the blends.[23] The relatively constant V_{oc} in the present P3BT:$PC_{61}BM$ blend photovoltaic devices is due to the constant optical bandgap of P3BT NWs in the blends. Thus, an important advantage of the P3BT NW approach to the BHJ solar cells is the stability of open circuit voltage.

The fill factor (FF) is another important parameter that affects the solar cell efficiency. The highest FF (0.56) of these P3BT:$PC_{61}BM$ blend solar cells was achieved at the highest $PC_{61}BM$ concentration of 67 wt % (33% P3BT); FF gradually decreased with the decreasing $PC_{61}BM$ fraction (Figure 9c) until 33% $PC_{61}BM$ and then dramatically decreased to 0.35 in $PC_{61}BM$ fraction of 20%. The variation in FF value may be explained by the different series and shunt resistances in the films with different compositions. The low P3BT concentration (33%) cell shows a more than doubled shunt resistance than the other cells, which compensates the reduction in FF because of a little higher series resistance, leading to the highest FF observed. From a concentration of 50 to 67%, the increase of the series resistance and the decrease of the shunt resistance result in the lowered FF. For the highest P3BT fraction (80%), the dramatically increased series resistance and the much lower shunt resistance account for the lowest FF among all the cells.

The power conversion efficiency (PCE) dependence on blend composition (Figure 9d) mirrors the short-circuit current density dependence on blend composition (Figure 9a), indicating that the PCE of the P3BT:$PC_{61}BM$ blend solar cells is dominated by the same factors as for J_{sc}. This can be understood by the relative stable V_{oc} in these P3BT:$PC_{61}BM$ blend solar cells. As is well-known, J_{sc} is the result of light absorption, exciton dissociation, and charge transport, which are also critical to the overall PCE. We note that unlike P3HT:$PC_{61}BM$ solar cells, in which the highest PCE was generally observed in the 1:1 blend composition,[23] the best performance among the present $PC_{61}BM$:P3BT NW solar cells was obtained from the 1:0.5 composition. It is advantageous to minimize the fullerene component because the fullerene contributes little to the light absorption. We note that further optimization of many variables, including the active layer thickness, annealing temperature and time, and even the blend composition, is necessary to improve the performance of polymer semiconductor nanowire-based BHJ solar cells.

(23) Kim, Y.; Choulis, S. A.; Nelson, J.; Bradley, D. D. C.; Cook, S.; Durrant, J. R. *J. Mater. Sci.* **2005**, *40*, 1371–1376.

Conclusions

The results of our study have demonstrated new bulk heterojunction P3BT:$PC_{61}BM$ photovoltaic cells created by an in situ self-assembly of P3BT nanowires as the donor component. The P3BT NWs, self-assembled in the presence of the fullerene acceptor, formed an interconnected network in the blend films. TEM and AFM imaging revealed P3BT NWs with 11−15 nm width and several micrometer length. High hole mobilities on the order of 1×10^{-3} cm^2/V s were observed in the P3BT nanowires/$PC_{61}BM$ nanocomposites by both SCLC and field-effect transistors. The photovoltaic properties, especially the short-circuit current density, fill factor, and power conversion efficiency were found to depend strongly on blend composition. A power conversion efficiency of 2.52% was achieved from the 1:0.5 P3BT:$PC_{61}BM$ blend in ambient air. The new in situ self-assembly approach provides a means for the rational control of the film morphology in bulk heterojunction polymer solar cells. The performance of the P3BT nanowire/$PC_{61}BM$ solar cells is mainly limited by the monomolecular recombination and the high series resistance, which should be addressed in future studies.

Acknowledgment. Our research was supported by the Department of Energy Basic Energy Sciences (DE-FG02-07ER46467), the NSF (DMR-0805259 and DMR-0120967), and in part by the AFOSR EHSS-MURI (FA9550-06-1-0326). Part of this work was conducted at the University of Washington NanoTech User Facility, a member of the NSF National Nanotechnology Infrastructure Network (NNIN).

CM801324M